Simulation of Heat and Water Transport on Different Tree Canopies: A Finite Element Approach

Carlos E. Villarreal-Olavarrieta [1] , Néstor García-Chan [2,*] and Miguel E. Vázquez-Méndez [3]

1   Departmento de Oceanografía Física, Centro de Investigación Científica y de Educación Superior de Ensenada, Ensenada 22860, Mexico; carloseduardo@cicese.edu.mx
2   Departamento de Física, CU de Cs Exactas e Ingeniería, Universidad de Guadalajara, Guadalajara 44430, Mexico
3   Departamento de Matemática Aplicada, Universidade de Santiago de Compostela, EPSE, 27002 Lugo, Spain; miguelernesto.vazquez@usc.es
*   Correspondence: nestor.gchan@academicos.udg.mx

Abstract: Heat and water transport modeling is a widely explored topic in micro-meteorology, agriculture, and forestry. One of the most popular models is the Simultaneous Heat and Water (SHAW) model, which includes partial differential equations (PDEs) for air-soil temperature and humidity, but with a priori discretized PDE for the foliage temperature in each canopy layer; it is solved using the finite difference method and the canopy shape is defined as a simple rule of proportionality of total quantities such as the total leaf area index. This work proposes a novel canopy shape characterization based on Weibull distribution, providing a continuous vertical shape function capable of fitting any tree species. This allows formulating a fully continuous SHAW-derived model, which is numerically solved by a finite element approach of P_1 Lagrange type. For this novel approach, several numerical experiments were carried out to understand how the shape of well distinguishable canopies influences heat and water transport.

Keywords: tree canopy; finite element method; Weibull distribution; SHAW model

1. Introduction

Forest and plant canopies have vertically varying profiles of different physical quantities related to complex transport processes. Variables as leaf temperature, water potential, wind velocity, longwave and shortwave radiation, photosynthesis, air and soil temperatures, but also the fluxes between soil-canopy-air have vertical profiles which change in function of the vertical distribution of the canopy biomass—mainly its leaves—(see the review by [1] and references therein). Such variability of physical properties deeply affects evapotranspiration and heat fluxes within the soil-vegetation-atmosphere system (SVAT).

To study complex processes within the canopy, mathematical models with a single homogeneous biomass layer —the so-called "big leaf" models—were used as a first approach. Later models were improved by including soil-vegetation-atmosphere heat and mass fluxes, and finally, multi-layer models arise as a more realistic choice as the vertical canopy shape is considered. However, the multi-layer models sometimes are not necessarily better; thus, model selection is subject to the scope of study [1]. This allows the formulation of different models, single or multi-layered, to study the different phenomena in forest and plants canopies, some of which are harmful to human life quality. Several examples could be enunciated: an evaluation of the radiation that reaches the soil and tree transpiration as means to mitigate the urban heat island (UHI) [2], a study of trees resistance to wind loads, and efficiency evaluation of trees as windbreakers [3], formulation of a multi-layer model to estimate the radiation distribution inside the canopy [4], use of a high-resolution model to study the water stress in a forest mulch layering [5], estimation of heat and water fluxes in the soil layer [6].

One of the well-known models is the Simultaneous Heat and Water (SHAW) model formulated by Flerchinger et al. [7] as a PDEs' model which has been updated several times [8–10], improving with it resolution associated with radiation, mass, sensible and latent heat fluxes, and recently [11] to model vertical profiles of temperature and humidity in a given tree canopy.

The SHAW model significantly depends on the leaf area index (LAI, a parameter that quantifies the canopy biomass) to model the leaf-air interchange of sensible heat and humidity. Frequently LAI is estimated merely as the total surface of leaves projected on a horizontal plane, known as total LAI, and holds no information about the vertical biomass distribution through the canopy [12]. The SHAW model requires a known value of LAI in each canopy layer, turning LAI in a priori discretized function; for example, in [11], this requirement is fulfilled with in situ measurements. This mandates a semi-discretized formulation of the SHAW model, leading to a finite difference scheme for its numerical resolution. Therefore, a continuous vertical function of LAI is needed for a continuous formulation of the SHAW model. The comments above lead us to focus on combining a continuous vertical canopy biomass profile with a multi-layer model to better approach vertical profiles of modeled state variables. As antecedents, in [13], the Weibull distribution is used successfully in curve fitting the leaf area density LAD—a vertical function of biomass canopy—of some tree species. On the other hand, in [14] a multi-layer, multi-species, and soil coupled model uses a continuous vertical function of LAD to upscale CO_2, water, heat, and momentum exchange from the canopy, validating the methodology with data from a tree canopy in Finland.

The accurate results shown in [14] suggest using a similar methodology to study —from a numerical point of view—the influence of the vertical canopy profile on the humidity and heat transport and air, leaf and soil temperatures. Therefore, in this paper, a SHAW-derived model is formulated in a fully continuous form (Section 2.1) using a continuous vertical profile of LAI drawn from the Weibull distribution (Section 2.2). After a detailed description of the initial and boundary conditions (Section 2.3), a combination of numerical techniques is proposed to solve the model (Section 2.4). It combines a finite element approach of P_1 Lagrange type for space discretization (a novelty in this kind of models), a finite difference scheme for time discretization, and a relaxed fix-point algorithm to address the resulting non-linear system. This method is applied in several numerical experiments where the resulting vertical profiles of leaf-air-soil temperatures, and humidity and heat fluxes corresponding to four different-shaped canopies showed notable variations (Section 3). Final remarks, discussions, and future work are presented in Section 4.

2. Materials and Methods

2.1. The Mathematical Model

In the model an air column with height h_a has within a tree canopy with height h_c and trunk height h_0 (then $0 < h_0 < h_c < h_a$). Furthermore, a soil layer with depth h_s is considered. Then we define the following sub-domains, the air column $\Omega_a = (0, h_a)$, the foliage layer of the canopy $\Omega_c = (h_0, h_c)$ and the soil layer $\Omega_s = (0, h_s)$. All of them are such that $\Omega_c \subset \Omega_a$ and $\Omega_s \cap \Omega_a = \emptyset$.

Now, we look for the state functions of air temperature $T_a(z, t)$, air humidity $p_v(z, t)$, leaf temperature $T_l(z, t)$, and soil temperature $T_s(z, t)$ such that satisfies the following nonlinear system of PDEs

$$\rho_a c_a \partial_t T_a = \partial_z [\rho_a c_a K_e \partial_z T_a + H_l(T_a, T_l)] \text{ on } \Omega_a \times [0, T] \tag{1a}$$

$$\partial_t p_v = \partial_z [K_e \partial_z p_v + E_l(p_v, T_l)] \text{ on } \Omega_a \times [0, T] \tag{1b}$$

$$m_c c_c \partial_z T_l = S_n + L_n - H_l(T_a, T_l) - L_v E_l(p_v, T_l) \text{ on } \Omega_c \times [0, T] \tag{1c}$$

$$\rho_s c_s \partial_t T_s = \partial_z (\lambda_s \partial_z T_s) \text{ on } \Omega_s \times [0, T] \tag{1d}$$

The mathematical model (1a)–(1d) is similar to the called Simultaneous Heat and Water (SHAW) model proposed by Flerchinger et al. [7,8] but not include a PDE related to soil humidity and Equation (1c) is continuous instead of discrete. The system incorporates air-canopy interchanges of sensible heat and humidity, absorbed shortwave and longwave net radiations, and assumes a well-mixed air column by turbulent transport. Consequently, the model needs complex empirical formulas, nonlinear coefficients, and correlations to define interchanges rates, resistances, friction velocity, and vertical wind profile. All of them are written down below as they were formulated in [7,8,11,15].

The turbulent transport coefficient K_e is given by the widely use K-theory

$$K_e = \begin{cases} ku_*(z - d + z_H)/\phi_H & z > d \\ ku_* z_H/\phi_H & z \leq d \end{cases} \tag{2}$$

being k the Von Karman constant, z_H the canopy height, $d \approx 0.77 h_c$ the zero-level displacement, ϕ_H is the dimensionless heat stability factor, and u_* the friction velocity given by

$$u_* = u_{ref} k \left[\ln \left(\frac{z_{ref} - d}{z_m} \right) + \psi_m \right]^{-1} \tag{3}$$

where u_{ref} is the reference wind speed at a given height z_{ref}.

This formulations of K_e and u^* are simple and commonly accepted in Micrometerology but has limitations. It draws constant transport coefficients below the zero displacement height d; the stability factor ϕ_H is calculated by sensible heat fluxes above the canopy; the effect of a sparse canopy and beyond the canopy could generate an undesirable damping effect [16,17]. Alternatives to address those limitations could be a non-parabolic approach for the free-surface layer given by a semi-theoretical coefficient of exponential type [17], the extended K-theory [18] or the called L-theory based on a Lagrangian point view of transport [16].

The interchange of sensible heat H_l and humidity E_l between air and canopy depends on the amount of foliage quantified by the leaf index area (LAI) as a vertical profile of the foliage mass, which will be defined later,

$$H_l = 2\rho_a c_a LAI \frac{T_l - T_a}{r_h} \tag{4a}$$

$$E_l = \begin{cases} LAI \frac{p_{vs} - p_v}{r_{ls} + r_v} & p_{vs} \geq p_v \\ 0 & p_{vs} < p_v \end{cases} \tag{4b}$$

The ideal gas law is used to estimate the humidity in the leaf stomata p_{vs} as a function of T_l,

$$p_{vs} = \frac{M_v}{RT_l} e_s(T_l) \tag{5}$$

where in turn M_v is the molecular mass of water, R the universal gas constant, and $e_s(T_l)$ is the water vapor pressure. Meanwhile, the interchange resistances to convective heat between air and leaf r_h, humidity between air and leaf r_v, and the evaporation in the leaf stomata r_{ls}, are all defined as

$$r_h = 7.4 \frac{\rho_a}{M_a} \sqrt{\frac{d_l}{u}} = 7.4 \frac{P}{RT_a} \sqrt{\frac{d_l}{u}} \tag{6a}$$

$$r_v = 6.8 \frac{\rho_a}{M_a} \sqrt{\frac{d_l}{u}} = 6.8 \frac{P}{RT_a} \sqrt{\frac{d_l}{u}} \tag{6b}$$

$$r_{ls} = \frac{r_{ls0}}{f_{S_t} f_T f_{VPD}} \left[1 + \left(\frac{\Psi_l}{\Psi_c} \right)^{n_s} \right] \tag{6c}$$

being u the wind profile, d_l the leaf characteristic length, P the atmospheric pressure, r_{ls0} the unstressed leaf interchange, Ψ_l the leaf water potential, Ψ_c the leaf critical water potential, and f_{St}, f_T, f_{VPD} are corrections on the stomata resistance to solar radiation, temperature and water vapor deficit, respectively. The wind profile has a logarithm profile above the canopy but exponentially decline in its interior

$$u = \begin{cases} \frac{u_*}{k}\left[\ln\left(\frac{z-d}{z_m}\right) + \psi_m\right] & z \geq h_c \\ \frac{u_*}{k}\left[\ln\left(\frac{h_c-d}{z_m}\right) + \psi_m\right] \exp\left(0.28\left(\frac{LAI_{tot}^2 h_c}{w_l}\right)^{1/3}\left(\frac{z}{hc} - 1\right)\right) & z < h_c \end{cases} \tag{7}$$

being u_* the friction velocity, z_m is the momentum transfer roughness, ψ_m is the diabatic momentum stability factor, w_l is the mean leaf width and LAI_{tot} is the total Leaf Area Index of the canopy. Again, the velocity profile (7) is classical and agree with the comments to Equation (2); there are alternatives, for example, in the free-surface beyond the canopy $z > h_c$, a non-parabolic profile proposed recently in [17].

Other relations needed for computing parameters related to atmospheric stability are:

$$\psi_H = \begin{cases} 4.7\zeta & \zeta \geq 0 \\ -2\ln\left(\frac{1 + \sqrt{1 - 16\zeta}}{2}\right) & \zeta < 0 \end{cases} \tag{8a}$$

$$\phi_H = \begin{cases} (1 - 16\zeta)^{-1/2} & \zeta \geq 0 \\ 1 + \frac{6\zeta}{1+\zeta} & \zeta < 0 \end{cases} \tag{8b}$$

being the atmospheric stability ζ given by

$$\zeta = \frac{k z_{ref} g H_\zeta}{\rho_a c_a T_a u_*^3} \tag{9}$$

with the total exchange of sensible heat formulated as

$$H_\zeta = \frac{k^2 \rho_a c_a u(z)[T_a(d + z_H) - T_a(z)]}{\left[\ln\left(\frac{z-d}{z_m}\right) + \psi_m\right]\left[\ln\left(\frac{z-d}{z_H}\right) + \psi_H\right]} \tag{10}$$

where $\psi_m = 0.6\psi_H$ for unstable conditions and $\psi_m = \psi_H$ for stable conditions.

Finally, L_n and S_n in (1c) represent the net longwave and shortwave radiations absorbed within the canopy, computed with a multi-layer model [4,9,15,19] (see Appendix A). To understand the effect of the canopy shape in the models' state variables, ideal conditions must be considered. Therefore, the soil layer has a water concentration constant along time, justifying eliminate the PDE related to soil humidity in the model. Moreover, the water vapor on leaf stomata is assumed to be saturated, implying that Equation (5) holds.

2.2. The Weibull Distribution and Canopy Shape Characterization

In the above subsection, the vertical interchange of heat and humidity between air and canopy depends on the amount of foliage quantified by LAI and —implicitly— of the foliage mass m_c. However, LAI and m_c are reported in field measurements as a 2D-flat projection, which in this work are called total leaf area index LAI_{tot} and total canopy biomass $m_{c,tot}$, respectively. So a vertical parametrization of both LAI and m_c is needed. Therefore this subsection defines them as the most straightforward continuous vertical functions using the well-known Weibull distribution, being so one of the main contributions of this work.

The Weibull distribution is a two-parameter distribution used widely in biology, meteorology, sciences materials, and others. It can be described by its probability density function $f(v)$ and its cumulative distribution function $F(v)$ as described in [20]:

$$f(v) = \frac{\beta}{\alpha}\left(\frac{v}{\alpha}\right)^{\beta-1}\exp\left(-\left(\frac{v}{c}\right)^{\beta}\right) \tag{11a}$$

$$F(v) = 1 - \exp\left(-\left(\frac{v}{c}\right)^{\beta}\right) \tag{11b}$$

where β is the Weibull module, α is the scale parameter and v is the independent variable. Is very important to note that $f(v)$ is the anti-derivative of $F(v)$ ($f(v) = F'(v)$). Applying these concepts to the tree canopy, another element to consider is the called leaf area density $LAD = LAD(z)$, a vertical shape function that quantified mass change concerning the canopy height. Assuming that $LAD(z)$ is known, we can relate it with different LAI definitions (see [13])

$$LAI_{tot} = \int_0^{h_c} LAD(z)\,dz \tag{12a}$$

$$LAI_a = \int_z^{h_c} LAD(s)\,ds \tag{12b}$$

being LAI_a the cumulative leaf area index. The shape function $LAD(z)$ can be adjusted by the following Weibulls' probability distribution [14,21,22]

$$LAD = LAI_{tot}\left(\frac{\beta_c}{\alpha_c}\left(\frac{1-z/h_c}{\alpha_c}\right)^{\beta_c-1}\exp\left(-\left(\frac{1-z/h_c}{\alpha_c}\right)^{\beta_c}\right)\right) \tag{13}$$

Similarly, the cumulative LAI_a is defined as the following Weibulls' cumulative distribution

$$LAI_a = LAI_{tot}\left\{1 - \exp\left[-\left(\frac{1-z/h_c}{\alpha_c}\right)^{\beta_c}\right]\right\} \tag{14}$$

where in both cases LAI_{tot} is taken as a proportionality constant. Defining $v = 1 - z/h_c$, we have that $LAD(v) = LAI'_a(v)$ holds, and LAI is computed straightforwardly in an arbitrary canopy layer of length $v_1 - v_0$ in the following way

$$LAI = \int_{v_0}^{v_1} LAD(v)\,dv = LAI_a(v_1) - LAI_a(v_0) \tag{15}$$

taking $v_1 = 1 - (z + \Delta z)/h_c$ and $v_0 = 1 - z/h_c$ as relative positions in the plant canopy, an useful expression of LAI in a canopy layer of length Δz is formulated as

$$LAI(z) = LAI_{tot}\left(\exp\left(-\left(\frac{1-z/h_c}{\alpha_c}\right)^{\beta_c}\right) - \exp\left(-\left(\frac{1-(z+\Delta z)/h_c}{\alpha_c}\right)^{\beta_c}\right)\right) \tag{16}$$

In a totally similar way, the biomass of the foliage m_c as a function of z could be formulated as

$$m_c(z) = m_{tot}\left(\exp\left(-\left(\frac{1-z/h_c}{\alpha_c}\right)^{\beta_c}\right) - \exp\left(-\left(\frac{1-(z+\Delta z)/h_c}{\alpha_c}\right)^{\beta_c}\right)\right) \tag{17}$$

being m_{tot} the total biomass in the canopy.

2.3. Initial and Boundary Conditions

In this subsection, the initial boundary conditions will be formulated. For this purpose, it must be noted that the model domain has three physical borders: soil ($z = h_s$), interface soil-air ($z = 0$) and air column height ($z = h_a$). There are no boundaries between the canopy and air; instead, there are interchanges of heat and water, which can be computed using the continuous function LAI (Equation (16)). Therefore, assuming that in an initial time the air temperature, leaf temperature, humidity and soil temperature are known the following initial conditions are imposed to the state variables of the model $T_a(.,0) = T_a^0(.)$, $p_v(.,0) = p_v^0(.)$, $T_l(.,0) = T_l^0(.)$ and $T_s(.,0) = T_s^0(.)$. Concerning the boundary conditions, a heat and humidity flux is assumed in the upper part of the air column ($z = h_a$), and the same in the lower part of the soil layer ($z = h_s$). Then, with knowing reference time functions $T_{a,ref}(t)$, $p_{v,ref}(t)$ and $T_{s,ref}(t)$, the following boundary conditions are imposed for all $t \geq 0$

$$\rho_a c_a K_e \partial_z T_a(h_a, t) = k_a(T_{a,ref}(t) - T_a(h_a, t)) \tag{18a}$$

$$K_e \partial_z p_v(h_a, t) = k_v(p_{v,ref}(t) - p_v(h_a, t)) \tag{18b}$$

$$\lambda \partial_z T_s(h_s, t) = k_s(T_{s,ref}(t) - T_s(h_s, t)) \tag{18c}$$

observing that for large value of the interchanges resistances $k_a, k_v, k_s \to \infty$, the previous conditions are transformed into the Dirichlet type conditions $T_a(h_a, t) = T_{a,ref}(t)$, $p_v(h_a, t) = p_{v,ref}(t)$ and $T_s(h_s, t) = T_{s,ref}(t)$.

Finally, in the border between the soil layer and the air column ($z = 0$), interchange of heat and water and soil heat balance are considered. Therefore we impose the following conditions,

$$\rho_a c_a K_e \partial_z T_a(0, t) = -H_g(T_a, T_s) \tag{19a}$$

$$K_e \partial_z p_v(0, t) = -E_g(p_v, T_s) \tag{19b}$$

$$\lambda_s \partial_z T_s(0, t) = S_{n,0} + L_{n,0} - H_g(T_a, T_s) - L_v E_g(p_v, T_s) \tag{19c}$$

where H_g and E_g are sensible heat and vaporization fluxes between air and soil, L_v is the heat of vaporization, $S_{n,0}$ and $L_{n,0}$ are the net shortwave and longwave radiation absorbed by the soil. These last quantities must consider the process, which begins when the radiation reaches the upper part of the canopy and downward until reaching the soil. Therefore, a multi-layer model is used to approach them (see Appendix A). To compute the air-soil fluxes H_g and E_g similar formulations those above (in the canopy) are used, then

$$H_g = \rho_a c_a \left. \frac{(T_s - T_a)}{r_s} \right|_{z=0} \tag{20a}$$

$$E_g = \begin{cases} \left. \dfrac{(p_{vg} - p_v)}{r_s} \right|_{z=0} & p_{vg} \geq p_v \\ 0 & p_{vg} < p_v \end{cases} \tag{20b}$$

where in turn p_{vg} is the water steam concentration in the soil surface and r_s is the soil resistance to convection [16], computed both by the following equations

$$p_{vg} = \left. \frac{M_v}{R T_s} e_s(T_s) \right|_{z=0} \tag{21a}$$

$$r_s = \frac{1}{u_* k} \left[\ln\left(\frac{z_{ref,s} - d_s + z_{H,s}}{z_{H,s}} \right) + \psi_H \right] \tag{21b}$$

where $z_{ref,s}$, d_s, $z_{H,s}$ are the reference height, zero displacement height and heat transfer roughness. As before, there are alternatives to the logarithm profile to estimate r_s, for example, which is derived from the extended K-Theory and introduced in [23].

2.4. Numerical Solution

2.4.1. Finite Element Approach

On the part of Equations (1a), (1b), (1d) the usual finite element treatment will be applied (see [24,25]); however, it must be observed that Equation (1c) has no spatial gradient, so requires an accurate time discretization instead, using finite differences [26]. To avoid tedious calculations and large formulations, a straightforward process is displayed in this subsection. Let the Sobolev spaces $V = H^1(\Omega_a)$ and $W = H^1(\Omega_s)$ and its $L^2(\Omega)$ inner product denoted by $\langle ., . \rangle$. Furthermore, the spacial domain $\Omega_a \cup \Omega_s$ is meshed using two meshes τ_a and τ_s, given by the partitions $h_a = z_{n_a} > z_{n_a-1} > \cdots > z_0 = 0$ and $0 = \hat{z}_0 > \hat{z}_1 > \cdots > \hat{z}_{n_s} = h_s$ with $n_a + 1$ and $n_s + 1$ nodes respectively. It is important consider the existence of a canopy mesh τ_c with $n_c + 1$ nodes covering the foliage layer $\Omega_c = (h_0, h_c)$ and such that $\tau_c \subset \tau_a$. Once the meshes are defined let be the discrete spaces $V_h = \{\varphi_h \in C(\bar{\Omega}_a) : \varphi_h|_{I_i} \in P_1(I_i)\}$ and $W_h = \{\hat{\varphi}_h \in C(\bar{\Omega}_s) : \hat{\varphi}_h|_{\hat{I}_i} \in P_1(\hat{I}_i)\}$ such that $V \approx V_h$ and $W \approx W_h$, then it is possible formulate the following semi-discrete problem: Find $(T_a, p_v, T_l, T_s) \in V_h \times V_h \times V_h \times W_h$ and $T_l \in \mathcal{C}(\Omega_c)$ such that for $\varphi_i \in V_h$ and $\hat{\varphi}_m \in W_h$ satisfies the following system equations

$$\langle \rho_a c_a \partial_t T_a, \varphi_i \rangle + \langle \rho_a c_a K_e \partial_z T_a, \varphi_i' \rangle + k_a\, T_a(h_a, t)\varphi_i(h_a) + k_{a0}\, T_a(0, t)\varphi_i(0)$$
$$= \langle \partial_z H_l, \varphi_i \rangle + k_a T_{a,ref} \varphi_i(h_a) + k_{a0} T_s(0, t)\varphi_i(0) \tag{22a}$$

$$\langle \partial_t p_v, \varphi_i \rangle + \langle K_e \partial_z p_v, \varphi_i' \rangle + k_v p_v(h_a, t)\varphi_i(h_a) + k_{v0} p_v(0, t)\varphi_i(0)$$
$$= \langle \partial_z E_l, \varphi_i \rangle + k_v p_{v,ref} \varphi_i(h_a) + k_{v0} p_{vg}(0, t)\varphi_i(0) \tag{22b}$$

$$m_c C_c \partial_t T_l = S_n + L_n - H_l - L_v E_l \tag{22c}$$

$$\langle \rho_s C_s \partial_t T_s, \hat{\varphi}_j \rangle + \langle \lambda_s \partial_z T_s, \partial_z \hat{\varphi}_j \rangle - k_s T_s(h_s, t)\hat{\varphi}_j(h_s)$$
$$= (S_{n,0} + L_{n,0} - H_g - L_v E_g)\hat{\varphi}_j(0) - k_s T_{s,ref} \hat{\varphi}_j(h_s) \tag{22d}$$

for each $i = 0, \ldots, n_a$; $j = 0, \ldots, n_s$ and being $k_{a0} = \frac{\rho_a c_a}{r_s}$, $k_{v0} = \frac{1}{r_s}$. Using the function basis for V_h and W_h is it possible to define over τ_a and τ_s the functions T_a, p_v, T_s, T_l as the following lineal combination

$$\Phi(z, t) = \sum_{j=0}^{n_x} \xi_j(t)\hat{\Phi}_j(z) \tag{23}$$

being $\xi_j(t) = \Phi(z_j, t)$ the time depend state variable and $\{\hat{\Phi}_j(z)\}_{j=0}^{n_x}$ the set of nodal basis functions. Thus, we define the following spacial discretized functions $\mathbf{T_a}(t) = \{\tilde{T}_{a,j}(t)\}_{j=1}^{n_a}$, $\mathbf{p_v}(t) = \{\tilde{p}_{v,j}(t)\}_{j=1}^{n_s}$, $\mathbf{T_s}(t) = \{\tilde{T}_{s,k}(t)\}_{k=1}^{n_s}$, and $\mathbf{T_l}(t) = \{\tilde{T}_{l,j}(t)\}_{j=n_0}^{n_a}$. From the initial conditions, we have known the vectors $\mathbf{T_a}(0) = \{T_{a,i}^0\}_{i=0}^{n_a}$, $\mathbf{p_v}(0) = \{p_{v,i}^0\}_{i=0}^{n_a}$, $\mathbf{T_s}(0) = \{T_{s,m}^0\}_{m=ns}^{0}$, $\mathbf{T_l}(0) = \{T_{l,i}^0\}_{i=n_0}^{n_c}$ which are the initial conditions for the following system of ordinary differential equations

$$\rho_a c_a \mathbf{M} \frac{d\mathbf{T_a}}{dt}(t) + [\mathbf{R_a} + \mathbf{B_a}]\mathbf{T_a}(t) = \mathbf{h_a}(t) + \mathbf{b_a}(t) \tag{24a}$$

$$\mathbf{M} \frac{d\mathbf{p_v}}{dt}(t) + [\mathbf{R_v} + \mathbf{B_v}]\mathbf{p_v}(t) = \mathbf{e_v}(t) + \mathbf{b_v}(t) \tag{24b}$$

$$C_c \mathbf{m_c} \frac{d\mathbf{T_l}}{dt}(t) = \mathbf{S_n}(t) + \mathbf{L_n}(t) - \mathbf{H_l}(t) - L_v \mathbf{E_l}(t) \tag{24c}$$

$$\mathbf{M_s} \frac{d\mathbf{T_s}}{dt}(t) + \mathbf{R_s}\mathbf{T_s}(t) = \mathbf{b_s}(t) \tag{24d}$$

where the contribution of 2×2 matrices and 2×1 vectors for arbitrary elements $I^l = [z_l, z_{l+1}]$ of τ_a and $\hat{I}^r = [\hat{z}_r, \hat{z}_{r+1}]$ of τ_s are given by

$$(\mathbf{M})_{i,l}^{l} = \langle \varphi_m, \varphi_l \rangle \tag{25a}$$

$$(\mathbf{R_a})_{i,j}^{l} = -\langle \rho_a c_a K_{e,j} \varphi_j', \varphi_i \rangle \tag{25b}$$

$$(\mathbf{B_a})_{i,j}^{l} = k_{La} \varphi_j(h_a) \varphi_i(h_a) + k_{a0} \varphi_j(0) \varphi_i(0) \tag{25c}$$

$$(\mathbf{h_a})_{i}^{l} = \langle \partial_z H_l, \varphi_i \rangle \tag{25d}$$

$$(\mathbf{b_a})_{i}^{l} = k_{a0} T_s(0,t) \varphi_i(0) + k_a T_{a,ref} \varphi_i(h_a) \tag{25e}$$

$$(\mathbf{R_v})_{i,j}^{l} = -\langle K_{e,j} \varphi_j', \varphi_i \rangle \tag{25f}$$

$$(\mathbf{B_v})_{i,j}^{l} = k_v \varphi_j(h_a) \varphi_i(h_a) + k_{v0} \varphi_j(0) \varphi_i(0) \tag{25g}$$

$$(\mathbf{b_v})_{i}^{l} = k_{v0} p_{vg}(0,t) \varphi_i(0) + k_v p_{v,ref} \varphi_i(h_a) \tag{25h}$$

$$(\mathbf{e_v})_{i}^{l} = \langle \partial_z E_l, \varphi_i \rangle \tag{25i}$$

$$(\mathbf{m_c})_{i}^{l} = m_c(z_i), \ (\mathbf{S_n})_{i}^{l}(t) = S_{n,i}, \ (\mathbf{L_n})_{i}^{l}(t) = L_{n,i} \tag{25j}$$

$$(\mathbf{M_s})_{m,k}^{r} = \langle \hat{\varphi}_k, \hat{\varphi}_m \rangle \tag{25k}$$

$$(\mathbf{R_s})_{m,k}^{r} = -\langle \lambda_s \hat{\varphi}_k', \hat{\varphi}_m \rangle + k_s \hat{\varphi}_m(h_s) \varphi_k(h_s) \tag{25l}$$

$$(\mathbf{b_s})_{k}^{r}(t) = (S_g + L_g - H_g - L_v E_g) \hat{\varphi}_k(0) + k_s T_{s,ref} \hat{\varphi}_k(h_s) \tag{25m}$$

for $i, j = l, l+1$, and $k, m = r, r+1$. The vectors $\mathbf{h_a}$ and $\mathbf{e_v}$ depend on nonlinear relations of temperature and humidity. Taking advantage of the 1D mesh and by simplicity, they are computed using a finite difference approach. A finite element approach is also possible, and it is formulated in Appendix B.

2.4.2. Time Discretization and Relaxed Fixed Point Scheme

As was the case in spatial discretization, the treatment of the system equations will not be the same. Therefore, Equations (24a), (24b), (24d) were time discretized using an Euler Backward scheme. Meanwhile, in Equation (24c), a bi-level type discretization with an Euler–Backward scheme was applied for the first level and a three-point derivative approach on the second level and higher, as is described in [26]. Therefore our problem is now: Given the initial vectors $\mathbf{T_a^0}$, $\mathbf{p_v^0}$, $\mathbf{T_s^0}$, $\mathbf{T_l^0}$ find the vectors $\mathbf{T_a^{n+1}}$, $\mathbf{p_v^{n+1}}$, $\mathbf{T_s^{n+1}}$, $\mathbf{T_l^{n+1}}$ such that for $n = 0, \ldots, N-1$ satisfies the following system

$$\rho_a c_a \mathbf{M} \frac{\mathbf{T_a^{n+1}} - \mathbf{T_a^n}}{\Delta t} + [\mathbf{R_a} + \mathbf{B_a}]\mathbf{T_a^{n+1}} = \mathbf{h_a^{n+1}} + \mathbf{b_a^{n+1}} \tag{26a}$$

$$\mathbf{M} \frac{\mathbf{p_v^{n+1}} - \mathbf{p_v^n}}{\Delta t} + [\mathbf{R_v} + \mathbf{B_v}]\mathbf{p_v^{n+1}} = \mathbf{e_v^{n+1}} + \mathbf{b_v^{n+1}} \tag{26b}$$

$$\left.\begin{array}{l} C_c \mathbf{m_c} \dfrac{\mathbf{T_l^{n+1}} - \mathbf{T_l^n}}{\Delta t} = \mathbf{G^{n+1}}, \quad n = 0 \\[2mm] C_c \mathbf{m_c} \dfrac{3\mathbf{T_l^{n+1}} - 4\mathbf{T_l^n} + \mathbf{T_l^{n-1}}}{2\Delta t} = \mathbf{G^{n+1}}, \quad n = 1, \ldots, N-1 \end{array}\right\} \tag{26c}$$

$$\mathbf{M_s} \frac{\mathbf{T_s^{n+1}} - \mathbf{T_s^n}}{\Delta t} + \mathbf{R_s} \mathbf{T_s^{n+1}} = \mathbf{b_s^{n+1}} \tag{26d}$$

being $\mathbf{G^{n+1}} = \mathbf{S_n^{n+1}} + \mathbf{L_n^{n+1}} - \mathbf{H_l^{n+1}} - L_v \mathbf{E_l^{n+1}}$.

The system above is nonlinear, so numerical methods such as Piccard iteration (Fixpoint), Newton–Galerkin, or others are needed to approximate the system solution. A first choice is the Piccard method due to its simplicity (it is derivative-free) and when it converges, it does to the solution. However, the complexity and different scales of the empirical formulas, nonlinear coefficients, and correlations could make that the fix-point fails. Anticipating this problem, a more robust variant of the Piccard method consisting of a bi-level iteration of type predictor-corrector was applied

$$\mathbf{u}^{q+1} = F(\mathbf{u}^q) \tag{27a}$$

$$\hat{\mathbf{u}}^{q+1} = \beta \mathbf{u}^{q+1} + (\beta - 1)\mathbf{u}^q \tag{27b}$$

being q the fix-point index, $\mathbf{u}^q = [\mathbf{T_a^q}, \mathbf{p_v^q}, \mathbf{T_l^q}, \mathbf{T_s^q}]$ the state variables vector, F the application derived at isolating the linear state variable in each equation of the system, β a relaxation parameter such that $0 < \beta \leq 1$, $\hat{\mathbf{u}}^{q+1}$ the relaxed fix-point, $\mathbf{u}^{q+1}$ the predicted fix-point and $\mathbf{u}^q$ the initial guess. The idea of this bi-level scheme is made $\beta \to 0$ as at least one state variable has slow convergence in the fixed-point iterations, imposing with it the same convergence velocity for all the state variables in the sense of the following error criteria [25]

$$\sqrt{\frac{(\mathbf{u}^{q+1} - \mathbf{u}^q)^2}{(\mathbf{u}^{q+1})^2}} < \epsilon \tag{28}$$

for a predefined tolerance ϵ.

2.5. Mesh Configuration, Adjustments, and Sensible Analysis

Several numerical experiments were conducted to evaluate the stability, convergence, and parameter sensitivity of the solution. Those experiences showed the need for adjustments in the sub-domains meshes and some parameters. Therefore this subsection is devoted to showing the mesh configuration and solution stabilization criteria.

The abrupt changes between air-foliage-soil suggest large heat and humidity gradients, so to forestall instability, a standard strategy is using no regular meshes. Therefore we maximize node concentration on the border of the different sub-domains. To this end, the following criteria are used to concentrate the nodes of τ_a in the interface air-soil and the upper part of the canopy,

$$z_i = \begin{cases} h_0 \left(\dfrac{i}{n_0 - 1} \right)^2 & 0 \leq z < h_0,\ 0 < i < n_0 \\[2mm] z_{i-1} + \dfrac{h_c - h_0}{n_c} & h_0 \leq z \leq h_c,\ n_0 \leq i < n_c + n_0 \\[2mm] h_c + (h_a - h_c)\left(\dfrac{i - NC - n_0 + 1}{n_a} \right)^2 & h_c < z \leq h_a \\[2mm] & n_c + n_0 \leq i < n_a + n_c + n_0 \end{cases} \tag{29}$$

and for τ_s these criteria concentrate the nodes in the interface between the soil and air,

$$z_{\hat{\imath}} = h_s \left(\frac{\hat{\imath}}{n_s - 1} \right)^2 \quad 0 \leq z < h_s,\ 0 \leq \hat{\imath} < n_s \tag{30}$$

The stomata resistance r_{ls} is stressed by solar radiation, temperature, and humidity. We made an adjustment substituted (6c) by a discrete function which is based on a minimum value of radiation and heat to stabilize the interchange between leaf and air

$$r_{ls,i} = \begin{cases} r_{ls0}, & \text{if } (S_{n,i} \geq S_{n,min}) \wedge (T_{l,i} > T_{l,min}) \wedge (p_{vs} > p_v) \\[1mm] r_{ls0} \dfrac{S_{n,min}}{S_{n,i}}, & \text{if } (S_{n,i} < S_{n,min}) \wedge (T_{l,i} > T_{l,min}) \wedge (p_{vs} > p_v) \\[1mm] \infty, & \text{if } (S_{n,i} = 0) \wedge (T_{l,i} < T_{l,min}) \wedge (p_{vs} \leq p_v) \end{cases} \tag{31}$$

Finally, for the initial condition for T_s is imposed a piecewise function which is lineal close to the interface soil-air and constant in-depth until $z = h_s$,

$$T_s(z_{\hat{\imath}}, 0) = \begin{cases} \left(\dfrac{T_{s,ref} - T_{a,ref}}{z_{bc}} \right) z_{\hat{\imath}} + T_{a,ref} & z_{\hat{\imath}} \leq h_{bc} \\[2mm] T_{s,ref} & z_{\hat{\imath}} > h_{bc} \end{cases} \tag{32}$$

being $h_{bc} < h_s$ the maximum depth of linearization.

3. Results

Numerical Experiments, Comparative between Different Artificial Canopies

We first define the values of the fixed parameters that characterize all the canopies considered in the numerical experiments and others parameters mentioned through this paper (see Table A1 of Appendix C). However, we emphasizing here the follow parameter values, air column height $h_a = 50$ m, canopy height $h_c = 3$ m, total leaf area index $LAI_{tot} = 3.25$, total foliage mass $m_{c,tot} = 10$ kg m^{-2}, leaves orientation coefficient $x_f = 1$, length $d_l = 0.08$ m, width $w_l = 0.03$ m and stomata resistance $r_{ls0} = 5$ s m^3 kg^{-1}. Furthermore, parameters related to turbulent transport and theoretical wind profile for the air column $z_{ref} = 50$ m, $z_H = 0.078$ m, d $= 0.77 \, h_c$ and soil resistance, roughness, and soil level displacement $z_{ref,s} = 1$ m, $z_{H,s} = 0.078$ m, $d_s = 0.001$ m which corresponds to grass [27]. In the boundary we impose Dirichlet type conditions with constant values of $T_{a,ref}$, $p_{v,ref}$ and $T_{s,ref}$, similarly for initial conditions with constants values for T_a^0, p_v^0 and T_s^0. Conversely, we define four different shape canopies using the Weibull distribution, holding all of them the same LAI_{tot} and $m_{c,tot}$. To do it, we use different combinations of the pair (α_c, β_c) (see Table 1 and Figure 1a). The intention is to define four distinguishable canopy shapes with maximum foliage concentration at the top, middle and low parts of the canopy. Additionally, a height-wise foliage concentration in the canopy is added as the last case (see Figure 1a).


(**a**) Different canopy shapes

(**b**) Wind profile

(**c**) Radiations forcing the model
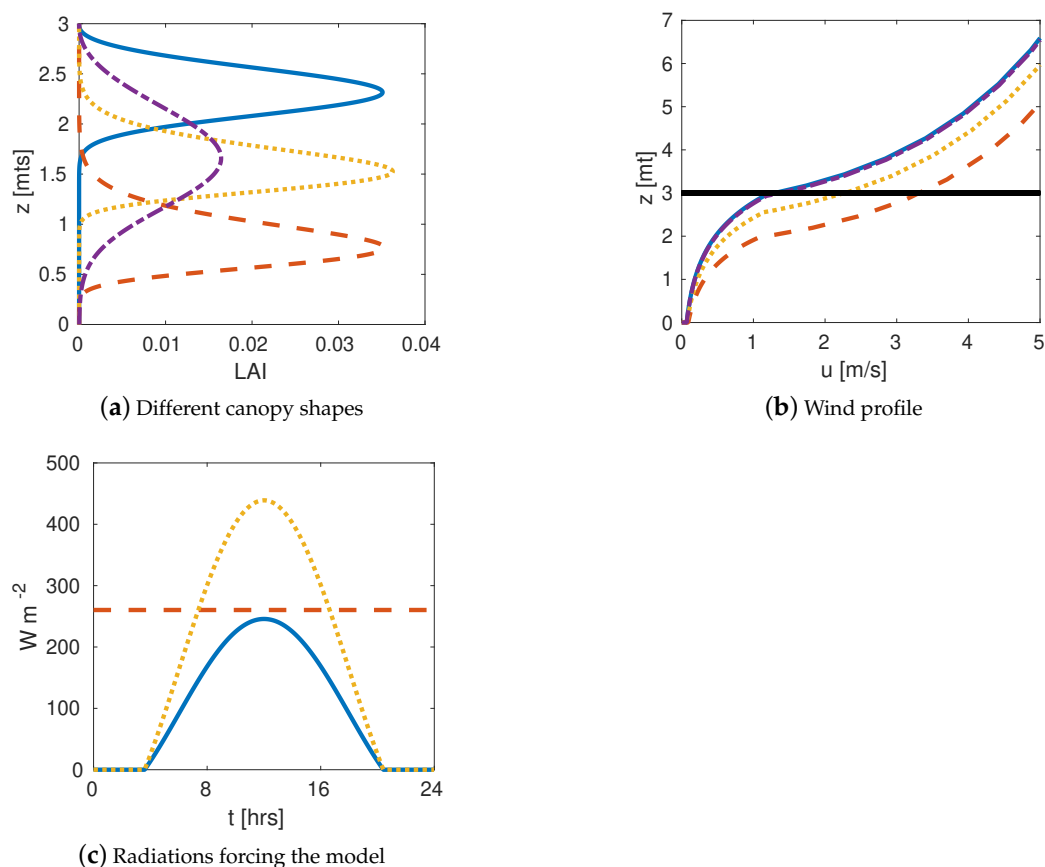
Figure 1. Inputs for the SHAW-derived model. (**a**) Different canopies shapes derived with the function $LAI(z)$ given by (13) and different combinations of the parameters pair (α_c, β_c). Cases, 1 (solid), 2 (dashed), 3 (dotted), and 4 (dash-dot). (**b**) Zoom of the Wind-profile for the four canopies shape, the black line is the canopy height. (**c**) 24 h radiation forcing from the sky at the upper layer in the canopy, Short wave-direct (solid), Short wave-diffusive (dotted), and Long wave-direct (dashed).

Table 1. Different pair values (α_c, β_c) of the parameters given to the Weibull distribution to define four distinguishable canopy shapes.

	Case 1 (Top)	Case 2 (Low)	Case 3 (Middle)	Case 4 (Height-Wise)
α_c	0.25	0.75	0.5	0.5
β_c	3.5	11.0	7.5	3.25

Between the inputs of the model, we have the vertical wind profile computed by Equation (7) and displayed in Figure 1b, including the line $h_c = 3\,\text{m}$, and the radiation forcing on the top of the canopy and shown in Figure 1c. Concerning the vertical profile of the wind, hold the decreasing values within the canopy and the exponential beyond it, noting that the interchange resistance coefficients (6a) and (6b) depends on wind speed. For radiation, diffusive and direct shortwave radiations reach their maximum at midday and are zero at night time. Meanwhile, the longwave radiation is set to be constant throughout the day, as it is dependent of the sky temperature.

Before showing the spatial-time evolution of the state variables, Figure 2 shows an approach of the thermal energy change in the canopy computing as $\Delta E = m_c\, c_c\, (T_l - T_{a,ref})$. As expected, the maximum energy change is located where is the maximum foliage mass position from the soil and where the wind velocity is minimum, being Case 2, which both conditions hold (Figure 2b). In contrast, the minimum energy change is a consequence of a foliage mass upper located from the soil and faster wind. In Case 1, both conditions hold with almost zero change (Figure 2a). Additionally, in all canopies (Figure 2), the foliage mass quantity on its limits is so slight that the thermal energy change is practically zero. This leads us to expect maximum leaf temperatures and quick humidity saturation at canopies' ends. However, these extremes values of temperature and humidity will be mitigated within the canopies. This is confirmed by the results explained and shown below.
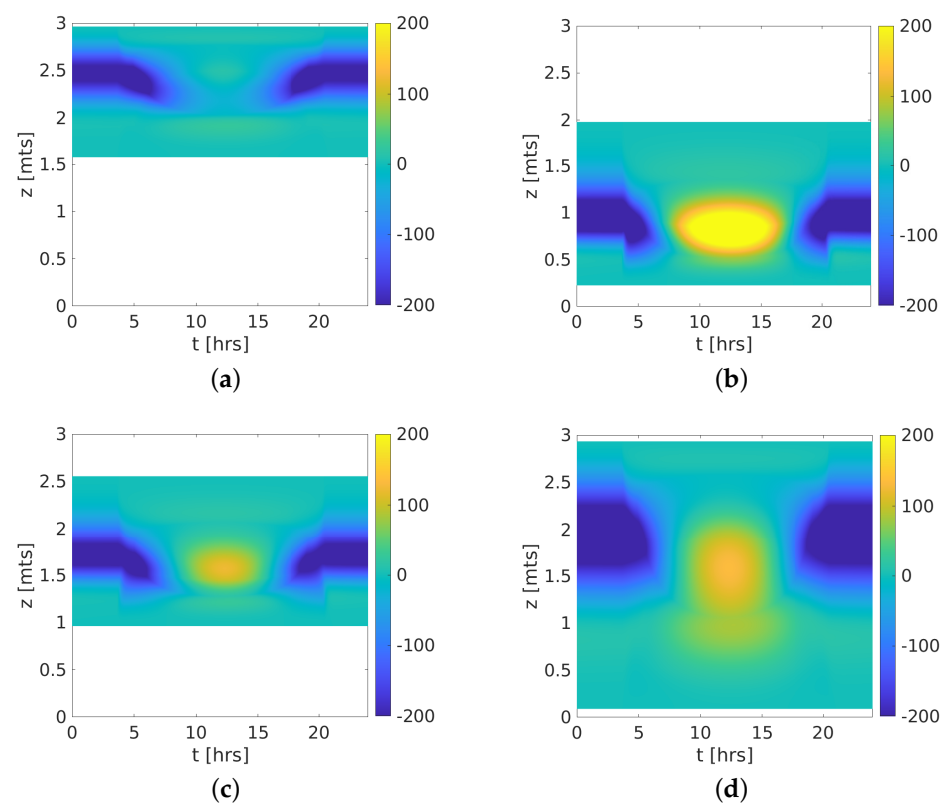
Figure 2. Energy change ΔE at 24 h for all canopy shapes. (**a**) Case 1; (**b**) Case 2; (**c**) Case 3; (**d**) Case 4.

We show in the following figures the space-time evolution of the state variables of the SHAW-derived model for all canopies. Numerical solutions have been computed in the mesh defined in Section 3 and a time interval of 24 h. As initial conditions to leaf-air-soil temperatures and leaf humidity were taken the outputs of a previous models' run of four days.

For the leaf temperature, Cases 1, 2, and 3 are all characterized by maximum temperatures on canopy ends due to minimum foliage mass and forcing by radiation from sky and soil (see Figure 3a–c). In particular, Case 4 shows notably more forcing on the low end of the canopy, in consequence, showing notably more significant temperature change there (due to a small foliage mass and a very short distance to the soil that radiates longwave energy and reflects part of the short wave radiation due to its albedo). Inside the canopy, the foliage mass allows moderate temperatures due to a significant net heat capacity.


(a)

(b)

(c)

(d)
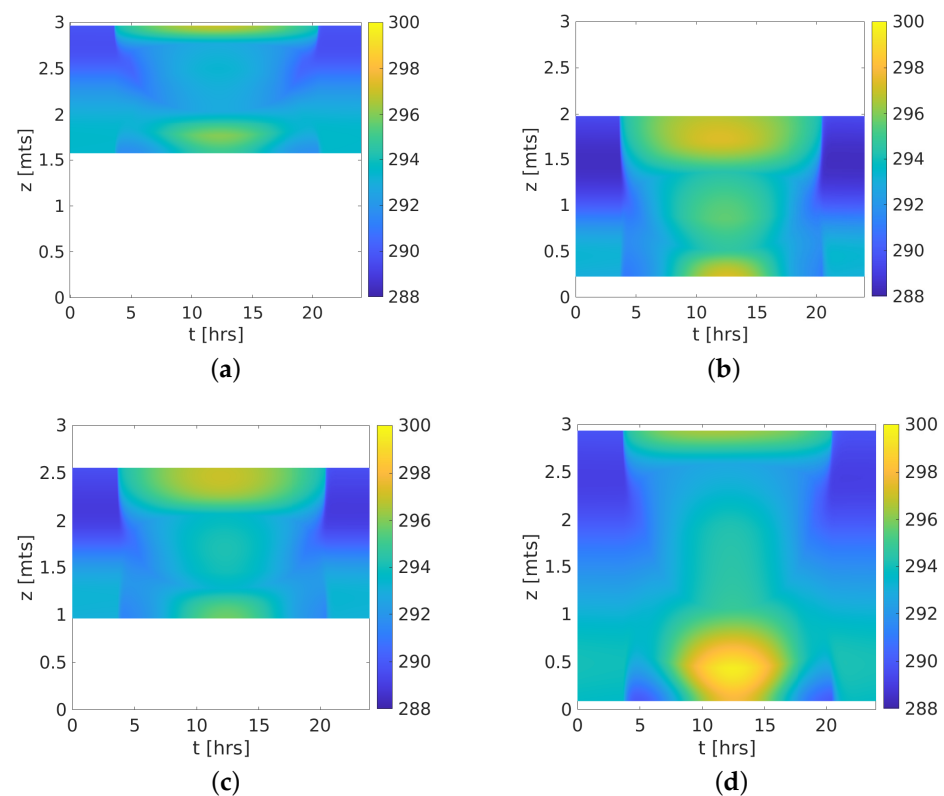
Figure 3. Leaf temperature variations at 24 h for all canopy shapes. (**a**) Case 1; (**b**) Case 2; (**c**) Case 3; (**d**) Case 4.

Now, the temperature of the air column is shown in Figure 4, taking only the part of the air column that matches the canopy height of 3 m. It is important to note that all canopies have the same temperature profile: maximum values close to the soil and decreasing through the canopy. We highlighted Case 2 (Figure 4a), which has a lower located foliage mass and higher energy change ΔE with air. In consequence, this canopy presents the maximum temperatures. Conforming the foliage mass is located in upper positions, the temperatures shown lower values due to a significant distance from the soil and less energy change capacity. Concerning Case 4, a well-mixed air temperature column (Figure 4d) is shown due to its height-wise foliage distribution. Nevertheless, all canopies show a scant variation ($\approx$0.4 K). This could be partly due to a high reference wind velocity $u_{ref} = 10$ m/s. To demonstrate that, we take lower velocity values $u_{ref} = 5$ m/s and $u_{ref} = 2.5$ m/s for Case 2, and results are shown in Figure 5a,b where a major variation ($\approx$1 K) is observed. There are others factors than potentially influence too, such as the constant temperature $T_{a,ref} = 293.15$ K imposed as boundary condition in the top of the air column and some parameters as the total biomass m_{tot}.
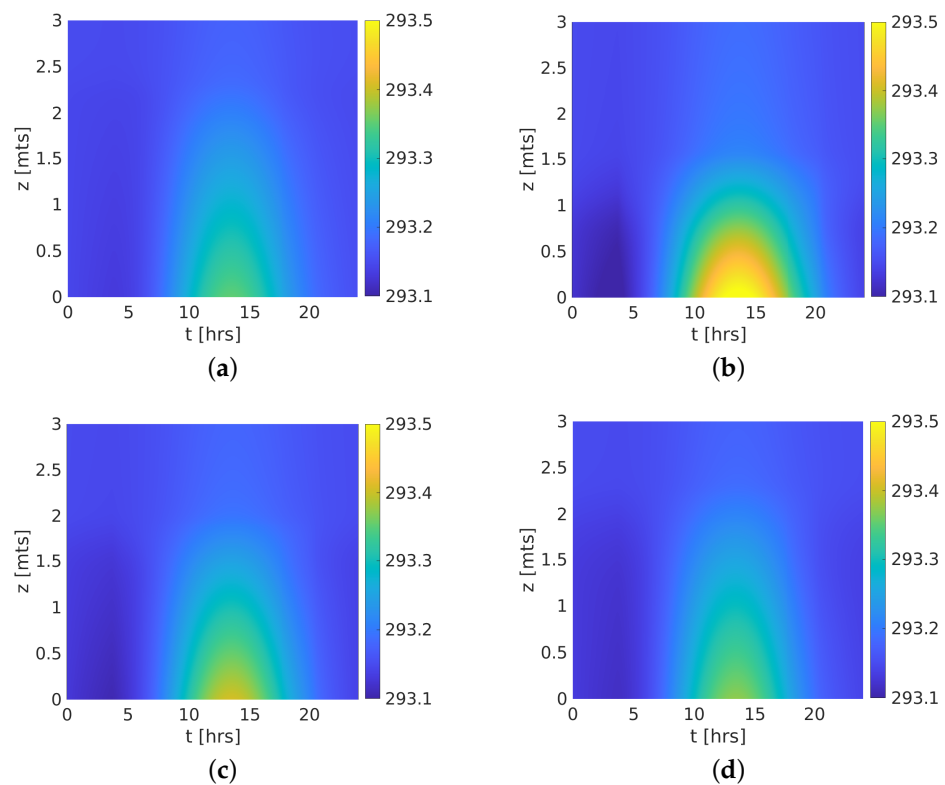
Figure 4. Air column temperatures at 24 h for all canopy shapes. (**a**) Case 1; (**b**) Case 2; (**c**) Case 3; (**d**) Case 4.
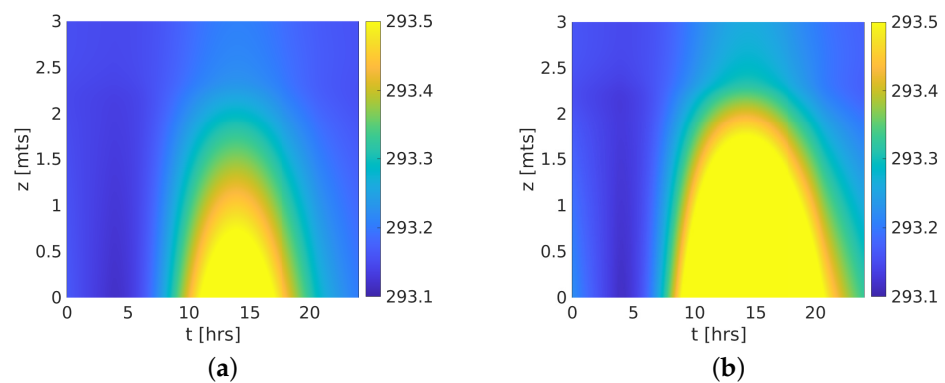

Figure 5. Wind velocity partly explains the scant variability of the temperature in the air column. Temperatures at 24 h for the canopy shape 2 subjected to different wind velocities. (**a**) Case 2 $u_{ref} = 5$ m/s; (**b**) Case 2 $u_{ref} = 2.5$ m/s.

About humidity, it is greatly influenced by the saturated soil (because of the more significant moisture flux in the soil-air inter-phase) is apparent the effect of the canopy shape, trapping, and adding (due to leaf stoma) humidity, avoiding its distribution along with the canopy. This can be observed clearly in opposites Cases 1 and 2 (Figure 6a,b) wherein the humidity line reaches 2.5 m in the first case, meanwhile only reaches 1.5 m in Case 1, matching with their respective canopies top.
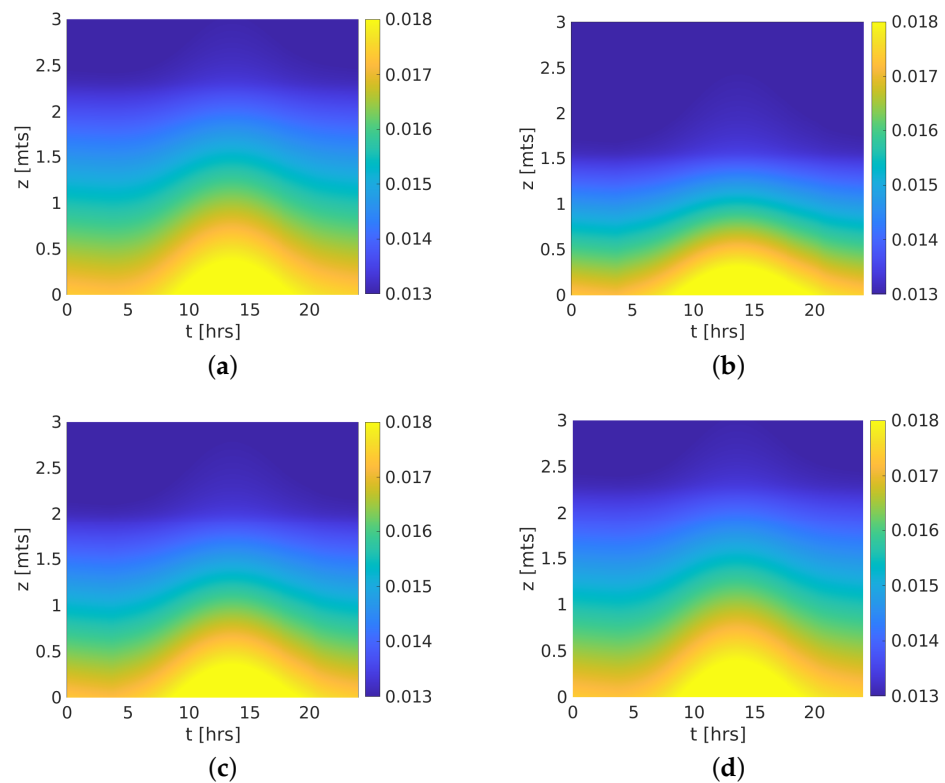
Figure 6. Leaf humidity at 24 h for all canopy shapes. (**a**) Case 1; (**b**) Case 2; (**c**) Case 3; (**d**) Case 4.

Finally, the soil temperature is computed from surface to a depth of -2 m but only presents a notable variation in a thick layer. Due to this, is shown only an average soil temperature. Then in Figure 7a is shown the average leaf temperature focuses our attention in the midday, wherein Case 2 (low foliage mass location) reaches the maximum temperature, opposite to its minimum corresponding to Case 1 (top foliage mass location). This indicates that to an upper location of the foliage, less soil temperature (due to a higher sensible heat soil cooling caused by steeper air and soil temperature difference).
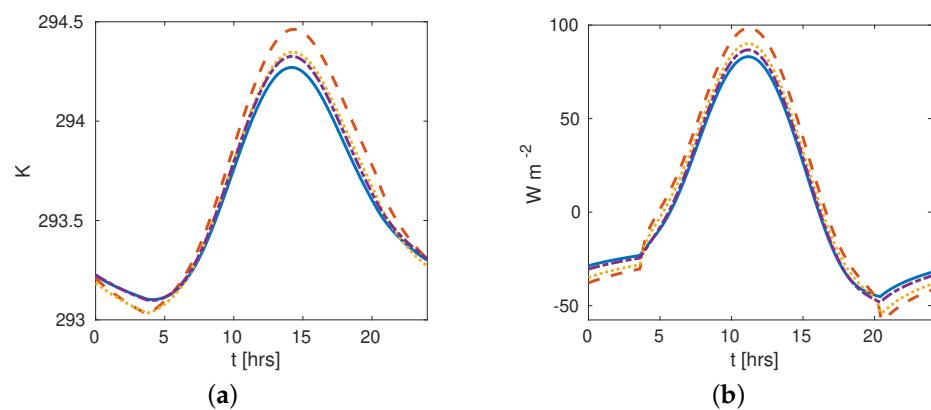
Figure 7. Temperature and heat balance in the soil, Cases 1 (solid), 2 (dashed), 3 (dotted), and 4 (dash-dot). In essence, the soil temperature and heat balance is the same for all the canopies, maximum values at midday and energy released at night. However, Cases 1 and 2 represent the extreme values from the rest of them. (**a**) Soil temperature (averaged in width); (**b**) Energy balance.

Of course, the model generates other interesting outputs: the net shortwave and longwave radiations in both soil and canopy. Energy fluxes at the soil surface (Equation (19c)) are shown in Figure 7b for all canopies. We expect that the canopy absorbs energy during the day and releases it at night. The shape canopy made a clear difference in magnitude of

released-absorbed energy with all canopies having the same exposed behavior. We point out that at midday, a difference of 20 Wm^{-2} between Cases 1 and 2, being the maximum and minimum values of the four cases.

4. Discussions

In this work, a SHAW-derived model was formulated and solved numerically with the finite element method, being an alternative to finite difference schemes used by Flerchinger et al. [7–11] and other authors (see reference list [28]). This new approach allows using irregular meshes and potentially scaling the model to a higher dimension which was possible thanks to the continuous vertical function LAI proposed in Section 2.2. Moreover, numerical solutions were derived by combining relaxed fix-point iterations (to address nonlinearity) and a time scheme of predicted-corrector type (to yield stability).

Typically, theoretical and experimental studies of heat and humidity fluxes in canopies are made on a fixed foliage profile either take it as a simple geometry shape —commonly triangular or rectangular— or derivate it by curve fitting of in situ measures. In this work, were compared different canopies characterized exclusively by their foliage profile or shape and analyzed their heat and water transport dynamics. Numerical results suggested that the canopy shape notably influences the vertical profile of leaf, air and soil temperatures, humidity and heat fluxes. Therefore, this work could be a first step in selecting a canopy tree to maximize its benefits. Examples could be several: windbreak, soil cooling or heating, reduced air temperature, maximized air humidity, covering the soil from radiation, and others. Furthermore, the simplicity of the Weibull distribution to characterize a canopy shape with only two parameters opens the possibility of formulating optimization problems related to minimizing harmful phenomenons.

We emphasize that the model could be sensitive to other canopy parameters: leaf width, orientation and diameter, stomata resistance, and specific heat capacity. Moreover, latitude, day of the year, and meteorological parameters are significant too. Therefore, changing these parameters would imply changes in the model outputs. However, address a model sensibility analysis would overextend this paper leaving it to future work.

A value-added of this work is a complete description of the mathematical methodology to obtain the numerical solution of the model, this could be attractive for researchers to reproduce results, update the model, or as another example of how to approach a nonlinear system of PDEs.

Finally, a comparison between the SHAW model and the SHAW-derived model (Equations (1a)–(1d)) could be interesting. However, there are essential differences between them: turbulent transport (K-theory), soil humidity, shape canopy characterization and numerical approach, which have been pointed out through the paper. Indeed, in [16] the substitution of the K-theory by the L-theory made a better approach of the modeled variables to the data. This motivates us to a model update for reach goals such as validation or model comparison. However, we do not consider this observations as a step backward but a direction for future work.

Appendix A. A Multi-Layer Model to Estimate the Radiation Extinction through the Canopy

Solar radiation is divided into long and shortwave radiation. Moreover, shortwave radiation is subdivided into diffusive or direct; longwave radiation is always diffusive. Moreover, the radiation could be downward or upward, reflected or absorbed. These radiation patterns are essential in the model, so this appendix shows how the amount of solar radiation in the canopy was estimated.

Let be the discrete functions $\{S_{d,j}\}_{j=1}^{n_c+1}$, $\{S_{b,j}\}_{j=1}^{n_c+1}$ the diffusive and direct radiation on each layer of the canopy, so in its upper part ($j = n_c + 1$)

$$S_{d,n_c+1} = \tau_{d,sky} I_{sky} \tag{A1}$$

$$S_{b,n_c+1} = \left(\tau_{t,sky} - \tau_{d,sky} \right) I_{sky} \tag{A2}$$

where $\tau_{d,sky}$ is the atmospheric coefficient of diffuse transmission, $\tau_{t,sky}$ is the maximum transmission at the clear sky and I_{sky} is the radiation reaching the upper section of the canopy. The detailed process to compute these parameters could be viewed in [29].

Once the radiation penetrates the canopy, an estimation of the absorbed radiation is needed. This is done by a multi-layer model [4,10,30], which divided the canopy into a finite number of layers, considering that one part of the radiation could pass to the following layer. Another part is reflected turn in diffusive downward and diffusive upward radiations. Therefore, let us consider the case of the short wave radiation, then for an arbitrary layer i, the direct radiation that passes between leaves is

$$S_{b,i} = \tau_{b,i} S_{b,i+1} \tag{A3}$$

meanwhile the diffuse downward radiation $S_{d,i}$ is given by

$$
\begin{aligned}
S_{d,i} = \ & \left[\tau_{d,i} + \left(\alpha_l f_{d,i,\downarrow\downarrow} + \tau_l f_{d,i,\downarrow\uparrow} \right) (1 - \tau_{d,i}) \right] S_{d,i+1} \\
& + \left(\alpha_l f_{b,i,\downarrow\downarrow} + \tau_l f_{b,i,\downarrow\uparrow} \right) (1 - \tau_{b,i}) S_{b,i+1} \\
& + \left(\alpha_l f_{d,i,\downarrow\uparrow} + \tau_l f_{d,i,\downarrow\downarrow} \right) (1 - \tau_{d,i}) S_{u,i-1}
\end{aligned}
\tag{A4}
$$

and the diffuse upward radiation $S_{u,i}$ is given by

$$
\begin{aligned}
S_{u,i} = \ & \left[\tau_{d,i} + \left(\alpha_l f_{d,i,\downarrow\downarrow} + \tau_l f_{d,i,\downarrow\uparrow} \right) (1 - \tau_{d,i}) \right] S_{u,i-1} \\
& + \left(\alpha_l f_{d,i,\downarrow\uparrow} + \tau_l f_{d,i,\downarrow\downarrow} \right) (1 - \tau_{d,i}) S_{d,i+1} \\
& + \left(\alpha_l f_{b,i,\downarrow\uparrow} + \tau_l f_{b,i,\downarrow\downarrow} \right) (1 - \tau_{b,i}) S_{b,i+1}
\end{aligned}
\tag{A5}
$$

where $f_{b,i,\downarrow\uparrow}$ and $f_{d,i,\downarrow\uparrow}$ are, respectively, the upward fraction of direct and diffusive radiation, $f_{b,i,\downarrow\downarrow}$ and $f_{d,i,\downarrow\downarrow}$ are, respectively, the downward fraction of direct and diffuse radiation, $\tau_{b,i}$ and $\tau_{d,i}$ are the percentage of direct and diffuse radiation which pass trough the gap between leaf; meanwhile, τ_l is the percentage of radiation which pass trough the leaves, and α_l is the leaf albedo (see [4,9,15,19]).

Finally, the upwards reflected radiation by the soil is computed as the reflected sum of the direct and diffuse radiations that reach the soil,

$$S_{u,0} = \alpha_s (S_{d,1} + S_{b,1}) \tag{A6}$$

and with this last equation, is completed the multi-layer model (A3)–(A6) for the shortwave radiation.

Once the system (A3)–(A6) is solved, the net short wave radiation absorbed by the canopy and soil is computed by the following conservative equations

$$S_{n,i} = (S_{b,i+1} + S_{d,i+1} + S_{u,i-1}) - (S_{b,i} + S_{d,i} + S_{u,i}) \tag{A7a}$$

$$S_{n,0} = S_{b,1} + S_{d,1} - S_{u,0} \tag{A7b}$$

With completely similar reasoning, the multi-layer model for the diffuse longwave radiation could be written. Therefore, the longwave radiation that reaches the upper part of the canopy ($j = n_c + 1$) is computed with the Stephan-Boltzman law

$$L_{d,n_c+1} = \epsilon_a \sigma T_{sky}^4 \tag{A8}$$

being ϵ_a the sky emissivity, σ the Stephan-Boltzman constant, T_{sky} the sky temperature in Kelvin and L_{d,n_c+1} the longwave radiation reaching the canopy.

On an arbitrary layer i of the canopy, the longwave radiation is divided in diffuse downward

$$
\begin{aligned}
L_{d,i} = {} & \left[\tau_{d,i} + (1 - \tau_{d,i})(1 - \epsilon_c) f_{d,i,\downarrow\downarrow} \right] L_{d,i+1} \\
& + (1 - \tau_{d,i})(1 - \epsilon_c) f_{d,i,\downarrow\uparrow} L_{u,i-1} \\
& + (1 - \tau_{d,i}) \epsilon_c \sigma T_{l,i}^4
\end{aligned}
\tag{A9}
$$

and diffuse upward

$$
\begin{aligned}
L_{u,i} = {} & \left[\tau_{d,i} + (1 - \tau_{d,i})(1 - \epsilon_c) f_{d,i,\downarrow\downarrow} \right] L_{u,i-1} \\
& + (1 - \tau_{d,i})(1 - \epsilon_c) f_{d,i,\downarrow\uparrow} L_{d,i+1} \\
& + (1 - \tau_{d,i}) \epsilon_c \sigma T_{l,i}^4
\end{aligned}
\tag{A10}
$$

meanwhile the longwave radiation absorbed by the soil is given by the balance

$$L_{u,0} = (1 - \epsilon_s) L_{d,1} + \epsilon_s \sigma T_{s,0}^4 \tag{A11}$$

being $T_{s,0}$ the ground surface temperature and ϵ_s the soil emissivity. This last equation completes the multi-layer model by the longwave radiation in the canopy (A9)–(A11).

Once the system (A9)–(A11) is solved, the net radiation absorbed by the canopy and the soil is given by the following conservative equations

$$L_{n,i} = L_{d,i+1} + L_{u,i-1} - (L_{d,i} + L_{u,i}) \tag{A12a}$$

$$L_{n,0} = L_{d,1} - L_{u,0} \tag{A12b}$$

Appendix B. Computing Contributions Matrices of the Gradients of E_l and H_l

We focus on two terms in the semi-discrete problem (22), which was approached by a finite difference scheme, is now listed as a finite element approach. We begin with $\langle \partial_z E_l, \varphi_i \rangle$, doing formal operations we have

$$\langle \partial_z E_l, \varphi_i \rangle = \left\langle \partial_z \frac{LAI}{r_{ls}+r_v}(p_{vs} - p_v), \varphi_i \right\rangle = \left\langle \partial_z \left(\frac{LAI}{r_{ls}+r_v} p_{vs} \right), \varphi_i \right\rangle - \left\langle \partial_z \left(\frac{LAI}{r_{ls}+r_v} p_v \right), \varphi_i \right\rangle \tag{A13}$$

being $p_{vs} = p_{vs}(T_l)$ a nonlinear relation and where p_v admits a representation as lineal combination, then we write

$$\left\langle \partial_z \frac{LAI}{r_{ls}+r_v}(p_{vs} - p_v), \varphi_i \right\rangle = \left\langle \partial_{z,j} \left(\frac{LAI}{r_{ls}+r_v} p_{vs}(\tilde{T}_{l,j}) \right), \varphi_i \right\rangle - \sum_{j=1}^{n_a} \eta_j \left\langle \partial_z \left(\frac{LAI}{r_{ls}+r_v} \varphi_j \right), \varphi_i \right\rangle \tag{A14}$$

now, taking an arbitrary element $I^i = [z_i, z_{i+1}]$ we compute its contribution to the system matrix

$$\left\langle \partial_z \left(\frac{LAI}{r_{ls}+r_v} \varphi_l \right), \varphi_m \right\rangle_{ml}^i = \int_{z_i}^{z_{i+1}} \partial_z \left(\frac{LAI}{r_{ls}+r_v} \varphi_l \right) \varphi_m \, dz = \frac{\overline{LAI}}{\overline{r_{ls}+r_v}} \int_{z_i}^{z_{i+1}} \varphi_l' \varphi_m \, dz$$

for $m, l = i, i+1$ and where $\overline{LAI}$, $\overline{r_{ls}+r_v}$ are the average on the element I^i. Given the value to sub-indexes m, l the follow contribution matrix is obtained

$$\mathbf{K_v}^i = \frac{\overline{LAI}}{\overline{r_{ls}+r_v}} \int_{z_i}^{z_{i+1}} \begin{bmatrix} -\varphi_i'\varphi_i & \varphi_{i+1}'\varphi_i \\ -\varphi_i'\varphi_{i+1} & \varphi_{i+1}'\varphi_{i+1} \end{bmatrix} dz = \frac{\overline{LAI}}{\overline{r_{ls}+r_v}} \begin{bmatrix} -1 & 1 \\ -1 & 1 \end{bmatrix}$$

On other part the first term at element I^i is computed as

$$\left\langle \partial_{z,j} \left(\frac{LAI}{r_{ls}+r_v} p_{vs}(\tilde{T}_{l,j}) \right), \varphi_i \right\rangle_m^i = \frac{\overline{LAI}}{\overline{r_{ls}+r_v}} \int_{z_i}^{z_{i+1}} \begin{bmatrix} \partial_z p_{vs}(\tilde{T}_l)\varphi_i \\ \partial_z p_{vs}(\tilde{T}_l)\varphi_{i+1} \end{bmatrix} dz$$

applying a forward-backward derivative approximation and a simple quadrature rule we have

$$\mathbf{k_v}^i = \frac{\overline{LAI}}{\overline{r_{ls}+r_v}} \int_{z_i}^{z_{i+1}} \begin{bmatrix} \partial_z p_{vs}(\tilde{T}_l)\varphi_i \\ \partial_z p_{vs}(\tilde{T}_l)\varphi_{i+1} \end{bmatrix} dz = \frac{\overline{LAI}}{\overline{r_{ls}+r_v}} \begin{bmatrix} \frac{\partial p_{vs,i}\varphi_{i,i}+\partial p_{vs,i+1}\varphi_{i,i+1}}{2}\Delta z \\ \frac{\partial p_{vs,i}\varphi_{i+1,i}+\partial p_{vs,i+1}\varphi_{i+1,i+1}}{2}\Delta z \end{bmatrix} =$$

$$\frac{\overline{LAI}}{\overline{r_{ls}+r_v}} \begin{bmatrix} \frac{p_{vs,i+1}-p_{vs,i}}{2} \\ \frac{p_{vs,i+1}-p_{vs,i}}{2} \end{bmatrix} = \begin{cases} \frac{\overline{LAI}}{2\overline{r_{ls}+r_v}}(p_{vs,i+1}-p_{vs,i})\begin{bmatrix} 1 \\ 1 \end{bmatrix} & p_{vs} \geq p_v \\ 0 & p_{vs} < p_v \end{cases} \tag{A15}$$

Respect to the second term $\langle \partial_z H_l, \varphi_i \rangle$ in the semi-discretized model (22), as above, with formal operations we have

$$\langle \partial_z H_l, \varphi_i \rangle = \left\langle \partial_z \left(\frac{2\rho_a c_a LAI}{r_h}(T_{l,j}-T_{a,j}) \right), \varphi_i \right\rangle$$

$$= 2\rho_a c_a \left[\left\langle \partial_z \left(\frac{LAI}{r_h} T_{l,j} \right), \varphi_i \right\rangle - \left\langle \partial_z \left(\frac{LAI}{r_h} T_{a,j} \right), \varphi_i \right\rangle \right]$$

$$= 2\rho_a c_a \sum_{j=1}^{n_a} \left[\xi_{l,j} \left\langle \partial_z \left(\frac{LAI}{r_h} \varphi_j \right), \varphi_i \right\rangle - \xi_{a,j} \left\langle \partial_z \left(\frac{LAI}{r_h} \varphi_j \right), \varphi_i \right\rangle \right] \tag{A16}$$

evaluating on arbitrary element $I^i = [z_i, z_{i+1}]$

$$\left\langle \partial_z \left(\frac{LAI}{r_h} \varphi_l \right), \varphi_m \right\rangle = \int_{z_i}^{z_{i+1}} \partial_z \left(\frac{LAI}{r_h} \varphi_l \right) \varphi_m dz = \frac{\overline{LAI}}{\overline{r_h}} \int_{z_i}^{z_{i+1}} \varphi_l' \varphi_m dz \tag{A17}$$

being $\overline{r_h}$ is an average resistance in the element. Using a simple quadrature rule and forward-backward derivative approximation

$$\mathbf{K_a}^i = 2\rho_a c_a \frac{\overline{LAI}}{\overline{r_h}} \int_{z_i}^{z_{i+1}} \begin{bmatrix} -\varphi_i'\varphi_i & \varphi_{i+1}'\varphi_i \\ -\varphi_i'\varphi_{i+1} & \varphi_{i+1}'\varphi_{i+1} \end{bmatrix} dz = \rho_a c_a \frac{\overline{LAI}}{\overline{r_h}} \begin{bmatrix} -1 & 1 \\ -1 & 1 \end{bmatrix}$$

therefore

$$\left\langle \partial_z \left(\frac{2\rho_a c_a LAI}{r_h}(T_{l,j}-T_{a,j}) \right), \varphi_i \right\rangle = \rho_a c_a \sum_{j=1}^{n_a} \left\{ \xi_{l,j} \frac{\overline{LAI}}{\overline{r_h}} \begin{bmatrix} -1 & 1 \\ -1 & 1 \end{bmatrix} - \xi_{a,j} \frac{\overline{LAI}}{\overline{r_h}} \begin{bmatrix} -1 & 1 \\ -1 & 1 \end{bmatrix} \right\}$$

Appendix C. Nomenclature and Values of the SHAW-derived Model Parameters

Table A1. Paremeter values used in the numerical experiences.

Symbol/Value	Definition	Symbol/Value	Definition
$t_f(h) = 24$ h	Simulation time	$L_v = 2.45 \times 10^6 \, \mathrm{J\,kg^{-1}}$	vaporization enthalpy
$c_a = 1004.5 \, \mathrm{J\,(kg\,K)^{-1}}$	specific heat air	$\rho_s c_s = 3.7 \times 10^6 \, \mathrm{J\,m^{-3}\,K^{-1}}$	soil conductivity
$c_c = 2200 \, \mathrm{J\,(kg\,K)^{-1}}$	specific heat foliage	$\lambda = 53.66^o$	latitude
$c_s = 3.77 \times 10^6 \, \mathrm{J\,(kg\,K)^{-1}}$	specific heat soil	$d = 0.77 h_c$	zero level displacemet
$d_l = 0.08$ m	characteristic leaf length	$d_s = 0.01$	soil level displacement
$d_n = 172$	day number of the year	$\tau_l = 0.35$	foliage transitivity
$h_a = 50$ m	air column height	$\Omega = 0.9$	pile leaves factor
$h_c = 3$ m	canopy height	$\tau_t = 0.6$	air transitivity
$h_s = 2$ m	soil layer width	$m_c = 10 \, \mathrm{kg\,m^{-2}}$	canopy biomass
$\alpha_s = 0.08$	soil albedo	$w_l = 0.03$ m	mean leaf width
$\alpha_c = 0.513$	foliage vertical profile	$\rho_a = 1.21 \, \mathrm{kg\,m^{-3}}$	air density
$\alpha_l = 0.15$	leaf albedo	$LAI_t = 2.25$	total LAI
$\epsilon_c = 0.90$	canopy emissivity	$r_{ls0} = 5 \, \mathrm{s\,m^{-1}}$	stomata resistance
$\epsilon_s = 0.94$	soil emissivity	$T_{sky} = 278.15$ K	sky temperature
$u_{ref} = 10 \, \mathrm{m\,s^{-1}}$	reference velocity	$T_{a,ref} = 293.15$ K	air reference temperature
$z_{ref} = 50$ m	reference height	$T_a^0 = 293.15$ K	initial air temperature
$z_{ref,s} = 1$	soil reference height	$T_l^0 = 280$ K	initial leaf temperature
$z_{H,s} = 0.001$	soil convection roughness	$T_{s,ref} = 293.0$ K	reference soil temperature
$n_a = 30$	mesh elements in air	$T_s^0 = 293.15$ K	initial soil temperature
$n_c = 500$	mesh elements in canopy	$\lambda_s = 2.9 \, \mathrm{J/(m\,K)}$	soil thermal conductivity
$n_s = 30$	mesh elements in soil	$\Delta t = 15$ s	time step
$n_0 = 25$	mesh elements in trunk	$p_{v,ref} = 0.013 \, \mathrm{kg/m^3}$	air reference humidity
$S_{n,min} = 0.5 \, \mathrm{W\,m^{-2}}$	minimum canopy radiation	$p_v^0 = 0.012 \, \mathrm{kg/m^3}$	initial humidity
$T_{l,min} = 277$ K	minimum stomata temperature		

References

1. Bonan, G.B.; Patton, E.G.; Finnigan, J.J.; Baldocchi, D.D.; Harman, I.N. Moving beyond the incorrect but useful paradigm: Reevaluating big-leaf and multilayer plant canopies to model biosphere-atmosphere fluxes—A review. *Agric. For. Meteorol.* **2021**, *306*, 108435. [CrossRef]
2. Yun, S.H.; Park, C.Y.; Kim, E.S.; Lee, D.K. A Multi-Layer Model for Transpiration of Urban Trees Considering Vertical Structure. *Forests* **2020**, *11*, 1164. [CrossRef]
3. Dargahi, M.; Newson, T.; Moore, J.R. A Numerical Approach to Estimate Natural Frequency of Trees with Variable Properties. *Forests* **2020**, *11*, 915. [CrossRef]
4. Zhao, W.; Qualls, R.J. A multiple-layer canopy scattering model to simulate shortwave radiation distribution within a homogeneous plant canopy. *Water Resour. Res.* **2005**, *41*. [CrossRef]
5. Wu, C.; Chau, K.; Huang, J. Modelling coupled water and heat transport in a soil–mulch–plant–atmosphere continuum (SMPAC) system. *Appl. Math. Model.* **2007**, *31*, 152–169. [CrossRef]
6. Banimahd, S.; Zand-Parsa, S. Simulation of evaporation, coupled liquid water, water vapor and heat transport through the soil medium. *Agric. Water Manag.* **2013**, *130*, 168–177. [CrossRef]
7. Flerchinger, G.; Pierson, F. Modeling plant canopy effects on variability of soil temperature and water. *Agric. For. Meteorol.* **1991**, *56*, 227–246. [CrossRef]
8. Flerchinger, G.N.; Kustas, W.P.; Weltz, M.A. Simulating Surface Energy Fluxes and Radiometric Surface Temperatures for Two Arid Vegetation Communities Using the SHAW Model. *J. Appl. Meteorol.* **1998**, *37*, 449–460. [CrossRef]
9. Flerchinger, G.; Yu, Q. Simplified expressions for radiation scattering in canopies with ellipsoidal leaf angle distributions. *Agric. For. Meteorol.* **2007**, *144*, 230–235. [CrossRef]
10. Flerchinger, G.; Xiao, W.; Sauer, T.; Yu, Q. Simulation of within-canopy radiation exchange. *NJAS-Wagening. J. Life Sci.* **2009**, *57*, 5–15. [CrossRef]
11. Flerchinger, G.N.; Reba, M.L.; Link, T.E.; Marks, D. Modeling temperature and humidity profiles within forest canopies. *Agric. For. Meteorol.* **2015**, *213*, 251–262. [CrossRef]
12. Coops, N.C.; Smith, M.L.; Jacobsen, K.L.; Martin, M.; Ollinger, S. Estimation of plant and leaf area index using three techniques in a mature native eucalypt canopy. *Austral Ecol.* **2004**, *29*, 332–341. [CrossRef]

13. Mori, S.; Hagihara, A. Crown profile of foliage area characterized with the Weibull distribution in a hinoki (Chamaecyparis obtusa) stand. *Trees* **1991**, *5*, 1432–2285. [CrossRef]

14. Launiainen, S.; Katul, G.G.; Lauren, A.; Kolari, P. Coupling boreal forest CO_2, H_2O and energy flows by a vertically structured forest canopy–Soil model with separate bryophyte layer. *Ecol. Model.* **2015**, *312*, 385–405. [CrossRef]

15. Campbell, G.S.; Norman, J. *An Introduction to Environmental Biophysics*; Springer Science + Business Media: New York, NY, USA, 1988. [CrossRef]

16. Flerchinger, G.N.; Reba, M.L.; Marks, D. Measurement of Surface Energy Fluxes from Two Rangeland Sites and Comparison with a Multilayer Canopy Model. *J. Hydrometeorol.* **2012**, *13*, 1038–1051. [CrossRef]

17. Absi, R. Reinvestigating the Parabolic-Shaped Eddy Viscosity Profile for Free Surface Flows. *Hydrology* **2021**, *8*, 126. [CrossRef]

18. Harman, I.N.; Finnigan, J.J. Scalar Concentration Profiles in the Canopy and Roughness Sublayer. *Bound.-Layer Meteorol.* **2008**, *129*, 323–351. [CrossRef]

19. Liu, R.; Huang, W.; Ren, H.; Yang, G.; Wang, J.; Li, X. Research on FPAR vertical distribution in different variety maize canopy. In Proceedings of the 2011 IEEE International Geoscience and Remote Sensing Symposium, Vancouver, BC, Canada, 24–29 July 2011; pp. 2745–2748. [CrossRef]

20. Lazzari, L. 8-Statistical Analysis of Corrosion Data. In *Engineering Tools for Corrosion*; Lazzari, L., Ed.; European Federation of Corrosion (EFC) Series; Woodhead Publishing: Kidlington, UK, 2017; pp. 131–148. [CrossRef]

21. Yang, X.; Witcosky, J.J.; Miller, D.R. Vertical Overstory Canopy Architecture of Temperate Deciduous Hardwood Forests in the Eastern United States. *For. Sci.* **1999**, *45*, 349–358. [CrossRef]

22. Coops, N.C.; Hilker, T.; Wulder, M.A.; St-Onge, B.; Siggins, A.; Trofymow, J.A. Estimating canopy structure of Douglas-fir forest stands from discrete-return LiDAR. *Trees* **1999**, *21*, 349–358. [CrossRef]

23. Oleson, K.W.; Lawrence, D.M.; Bonan, G.B.; Flanner, M.G.; Kluzek, E.; Lawrence, P.J.; Levis, S.; Swenson, S.C.; Thornton, P.E.; Dai, A.; et al. *Technical Description of Version 4.0 of the Community Land Model (CLM)*; Technical Report; National Center for Atmospheric Research: Boulder, CO, USA, 2010.

24. Larson, M.G.; Bengzon, F. *The Finite Element Method: Theory, Implementation, and Applications*; Springer: Berlin/Heidelberg, Germany, 2013. [CrossRef]

25. Reddy, J.N. *An Introduction to Nonlinear Finite Element Analysis with Applications to Heat Transfer, Fluid Mechanics, and Solid Mechanics*, 2nd ed.; Oxford University Press: Oxford, UK, 2014. [CrossRef]

26. Nakamura, S. *Applied Numerical Methods with Software*; Prentice-Hall: Harlow, UK, 1991; ISBN 9780130410474.

27. Hansen, F.V. *Surface Roghness Lengths*; Technical Report; U.S. Army Research Laboratory: Adelphi, MD, USA, 1994.

28. SHAW Model: USDA ARS. 2021. Available online: https://www.ars.usda.gov/ARSUserFiles/20520500/SHAW/302/SHAWReferences.pdf\T1\textquoteright (accessed on 4 February 2021).

29. Iqbal, M. *An Introduction to Solar Radiation*; Academic Press Canada: Waterloo, ON, Canada, 1983. [CrossRef]

30. Zhao, W.; Qualls, R.J. Modeling of long-wave and net radiation energy distribution within a homogeneous plant canopy via multiple scattering processes. *Water Resour. Res.* **2006**, *42*. [CrossRef]